Role of relaxation and time-dependent formation of x-ray spectra

Timofei Privalov, Faris Gel'mukhanov, and Hans Ågren
Theoretical Chemistry, Royal Institute of Technology, S-10044 Stockholm, Sweden
(Received 28 March 2001; published 8 October 2001)

A fundamental problem of x-ray spectroscopy is the role of relaxation of the electronic subsystem in the field of the transient core hole. The main intention of the present study is to explore the dynamics due to core-hole relaxation in the whole time domain, and to find out how it is manifested in finite molecular systems in comparison with solids. A technique is developed based on a reduction of the Noziéres-De Dominicis equation to a set of linear algebraic equations. The developed time-dependent formalism is applied to a numerical investigation of a one-dimensional tight-binding model. The formation of the x-ray profiles is explored on the real time scale, and the role of interaction with the core hole, band filling, and the final-state rule are investigated for systems of different size. The formation of spectra of the infinite translational invariant system is studied by extensions of the finite systems. We found that the dynamics of finite systems, like molecules, differs qualitatively from solids: Contrary to the latter the time lapse of the Noziéres-De Dominicis domain for finite systems is squeezed between the inverse bandwidth and the revival time, which is proportional to the system size. For small molecules this means that there is no time for a ''Mahan-Noziéres-De Dominicis singularity'' to develop. Comparison with the strict solution of the Noziéres-De Dominicis equation shows that the adiabatic approximation describes x-ray absorption and emission considerably better than the fast approximation. This explains the suppression of the relaxation effects in x-ray emission of, e.g., gas phase and surface adsorbed molecules, but also that these effects are essential for the absorption case. There is still a quantitative distinction between the adiabatic approximation and the strict approach, which becomes more important for larger systems. Adopting the so-called finite state rule by von Barth and Grossman also for molecules, an almost complete numerical agreement between this rule and the strict x-ray-absorption and emission profiles for systems of different sizes is obtained. The simulations indicate that the final-state rule correction is important mainly near the absorption edge and at the top of the emission band.

DOI: 10.1103/PhysRevB.64.165115 PACS number(s): 78.70.Ck, 32.30.Rj, 31.70.Hq

I. INTRODUCTION

X-ray spectroscopy constitutes a set of powerful experimental techniques to obtain insight into the nature of elementary excitations of molecules and condensed species. The worldwide development of synchrotron-radiation sources has during the 1990s created a breakthrough in this field nearly analogous to the one with laser sources in the optical region some 40 years ago. Even if this development has switched over much of the research emphasis to the resonant x-ray spectroscopies, the nonresonant counterparts have taken advantage of these modern synchrotron facilities as well.

The revival of x-ray spectroscopy has brought about new implications and applicabilities in molecular and material science for typical x-ray concepts like element, positional and polarization specificity, local bond and orientational probing, building-block principles, and chemical shifts. However, two interrelated conceptual issues remain with as great a concern as ever, namely, the role of relaxation in the formation of x-ray spectra and the extent to which the x-ray spectrum relates to the ground-state species. Since the x-ray spectra connect to core-electron excited states, the chemical and physical properties of which completely differ from those of the ground state (cf. the equivalent cores notion), these issues are of real concern for the main applicability of x-ray spectroscopy. The fundamental questions in this field thus refer to the role of the core hole in the formation of the spectral profile, and much efforts with so-called initial and final-state rules, with simplifying models and with large-scale computations have been devoted to find out for which type of systems and for which type of processes relaxation is important or not. One has thus found indication that relaxation in most cases is important for x-ray absorption, while, e.g. resonant inelastic x-ray scattering spectra of surface adsorbate species are best described by the frozen orbital approximation.[1]

However, the *a posterori* fact of whether experimental agreement is obtained with or without relaxation provides rather limited insight and predictability of the issue. Moreover, the direct connections between the role of relaxation with relevant concepts like detuning, band filling, and channel interference, and with processes for spectral formation that occur at different time scales—such as relaxation time, decay time, measurement time, and duration time—are not easily obtained using common time-independent computational methods. In order to better accomplish this ambition we believe a nonstationary, time-dependent framework for analysis and computations of the x-ray spectra is the one to look for. Time-dependent techniques have indeed been extremely fruitful for studying fundamental processes associated to the *nuclear* dynamics of x-ray spectra,[2] giving impetus to accomplish the similar picture for the electronic part of the problems.

To find a key and a starting point for this program we go back to Mahan's prediction of the edge singularities in x-ray spectra of metals,[3] and to the discovery by Noziéres and De Dominicis[4] (ND) that the core-hole problem is reduced, in a certain sense, to a one-electron problem in the Fermi-liquid

framework. Two distinct approaches were used to numerically solve this equation for solids: the direct solution of the time-dependent ND equation[5] and the solution of the ND equation in an energy representation.[6,7] Other theoretical machineries have been proposed as reviewed in Refs. 8–10. The ND theory, which contains an explicit treatment of the interaction with a core hole, admits a strict solution only near the threshold, while only numerical solutions are enabled in the whole spectral region. Thus, while the ND theory undisputably was a great breakthrough for the knowledge of the dynamics of an electronic system in the field of a core hole, it is limited to infinite systems and gives the analytical solution only for the long-time asymptote. The evolution of the electronic subsystem in the whole time domain, including also finite systems, has continued to be an open question, and to our knowledge a theory based on such a strict solution of the ND equation has never been implemented.

A key problem in the theory of x-ray spectra, and a goal of the present work, is thus a search of methods for a strict solution of the ND equation in the whole time domain. The present paper derives such a time-dependent method and addresses several issues concerning core-hole relaxation and interaction within the Fermi-liquid framework. The technique developed here to solve the ND equation is based on the reduction of the integral ND equation to linear algebraic equations and is adapted also for finite systems. Using this technique the spectra of infinite systems is computed as an extension of the size of the finite system. We test our formalism by applications to several main x-ray spectroscopies: x-ray absorption (XA), nonresonant x-ray emission (XE), and x-ray photoelectron spectroscopy (XPS), with the ambition to implement a similar technique in a more complicated many-body treatment for resonant x-ray Raman scattering. That will be the subject of a forthcoming paper.[11] We use the formalism to explore the appearance of x-ray spectra versus the strength of interaction with the core hole, versus band filling, and versus the time of interaction with the radiation. A special accent is also made on the role of excitonic states and on the applicability of the final-state rule[12] for finite systems.

The content of the paper is as follows. The basic ND theory of x-ray photoabsorption is described in the next section. Section III addresses our main result, the reduction of the time-dependent ND equation to an algebraic problem. The different limiting cases and the role of the band filling are discussed in Secs. III A and III B. We implement in Secs. IV and V the developed formalism to nonresonant x-ray emission and core-electron photoelectron spectra. The excitonic enhancement of many electron transitions is discussed in Sec. VI. Sections VII and VIII embody the details of numerical simulations and the discussion of the applicability of the final-state rule to the finite systems. The characteristic times of the electron dynamics and the time evolution of the XA, XE, and XPS profiles are studied in Sec. VIII E. Our findings are summarized in the last section.

II. BACKGROUND THEORY OF X-RAY ABSORPTION

We consider K photoabsorption with the photon $(\omega,\mathbf{e})$ and the dipole operator $\mathcal{D}_n=\Sigma_i(\mathbf{e}\cdot\mathbf{d}_{in})a_i^\dagger b_n$. Here b_n and $a_i^\dagger$ are the operators of annihilation of the core electron and creation of a valence electron, respectively. It is natural to express the wave function of the valence electron as a sum of the atomic orbitals ϕ_n,

$$\psi_i=\sum_n c_{in}\phi_n, \quad \sum_i |c_{in}|^2=\sum_n |c_{in}|^2=1, \tag{1}$$

which for simplicity are assumed to be nonoverlapping. A localization of the wave function of the $1s_n$ electron near the absorbing atom n results in the following expressions for the electron-hole interaction and the transition matrix element:

$$u_{ij}^n=c_{in}^*c_{jn}u_n, \quad (\mathbf{e}\cdot\mathbf{d})_{in}=c_{in}^*d, \tag{2}$$

where $d=\int\phi_n^*(\mathbf{e}\cdot\mathbf{r})1s_n d\mathbf{r}$. It is worthwhile to note that the readjustment of the Fermi sea in the field of the core hole suppresses strongly the coupling strength,[13] $u_n=(\phi_n 1s_n|\phi_n 1s_n)>0$.

We start out from the time-dependent representation for the cross section of x-ray K absorption, which is the sum of the contributions from each absorbing atom n,

$$\sigma(\omega)=\sum_n \sigma_n(\omega),$$

$$\sigma_n(\omega)=4\pi\alpha\omega\,\mathrm{Re}\int_0^\infty dt\langle 0|\mathcal{D}_n^\dagger(t)\mathcal{D}_n(0)|0\rangle e^{(\imath\omega-\Gamma)t}$$

$$=4\pi\alpha\omega|d|^2\,\mathrm{Re}\int_0^\infty dt e^{(i\omega-\Gamma)t}K_n(t-0,t). \tag{3}$$

Here $\alpha=\frac{1}{137}$. The cross section takes the form of a half-Fourier transform of the two-electron propagator

$$K_n(\tau,t)=\sum_{ij} c_{in}^*c_{jn}\langle 0|T\{b_n^\dagger(t)a_j(\tau)a_i^\dagger(0_+)b_n(0)\}|0\rangle,$$

$$0<\tau<t, \tag{4}$$

with $A(t)=\exp(\imath Ht)A\exp(-\imath Ht)$ and Γ is the lifetime broadening of the core excited state. The basic ND assumption of noninteracting valence electrons yields the following electronic Hamiltonian (see Appendix A):

$$H=\sum_i \epsilon_i a_i^\dagger a_i+\overline{E}_n b_n^\dagger b_n-\sum_{ij} u_{ij}^n a_i^\dagger a_j b_n b_n^\dagger,$$

$$\tilde{E}_n=E_n+u_n\sum_{i>F}|c_{in}|^2. \tag{5}$$

We use notations ϵ_i and E_n for the Hartee-Fock (HF) energies of valence and core electrons, respectively. The symbol $i>F$ means that the ith one-electron level is unoccupied and vice versa. We emphasize here one qualitative distinction of the valence and core-electron contributions to the Hamiltonian (5): contrary to the energy ϵ_i of the valence electron, $\overline{E}_n\equiv\tilde{E}_n-u_n$ is not equal to the HF value E_n. The often used identification of $\overline{E}_n$ and E_n is thus incorrect, for example, it results in a violation of the Manne-Åberg (MÅ) theorem[14,15]

(Secs. IV and VII, and Ref. 8). Obviously, $\overline{E_n}$ and E_n differ strongly due to the sharp dependency of $\overline{E_n}$ (5) on the filling of the valence band.

A key step is the profound idea of Noziéres and De Dominicis[4] to treat the core hole as a nonstationary classical scattering center switched on during the time lapse $[0,t]$ (but not as a particle). Due to this the correlator $K_n(\tau,t)$ factorizes into the product of the one-electron Green's functions for valence $[\varphi_n(\tau,t)]$ and core $(g_n(t)=-\iota\langle 0|Tb_n(0)b_n^{\dagger}(t)|0\rangle)$ electrons,

$$K_n(\tau,t)=\varphi_n(\tau,t)g_n(t). \tag{6}$$

The diagrammatic technique[4] or the equation-of-motion formalism[16] leads to the ND equations

$$\varphi_n(\tau,t)=G_n(\tau)-u_n\int_0^t G_n(\tau-\tau_1)\varphi_n(\tau_1,t)d\tau_1,$$

$$g_n(t)=\iota\theta(t)e^{[i\tilde{E}_n t+\Delta_n(t)]},\quad \Delta_n(t)=u_n\int_0^t \varphi_n(0_+,t_1)dt_1. \tag{7}$$

When the interaction with the core hole is neglected, $\varphi_n(\tau,t)$ coincides with the free-particle Green's function $G_n(\tau)=\theta(\tau)G_n^{+}(\tau)+\theta(-\tau)G_n^{-}(\tau)$. This results in a Hartree-Fock expression for the cross section (3). Here $\theta(\tau)$ is the step function, which is equal to one when $\tau>0$ and 0 otherwise, $G_n^{\pm}(\tau)=\pm\iota\Sigma_i|c_{in}|^2\theta[\pm(\epsilon_F-\epsilon_i)]\exp(-\iota\epsilon_i\tau)$, and ϵ_F is the Fermi energy.

III. REDUCTION OF THE ND EQUATION TO LINEAR ALGEBRAIC EQUATIONS

First of all we perform a Fourier transform of the ND equation (7) and extract the free-electron Green's function,

$$\varphi_n(\epsilon,t)=G_n(\epsilon)\tilde{\varphi}_n(\epsilon,t)=\int_{-\infty}^{\infty}d\tau e^{\iota\epsilon\tau}\varphi_n(\tau,t). \tag{8}$$

It is instructive to write the Fourier-transformed ND equation (see Appendix B),

$$[1+u_n\,\mathrm{Re}\,G_A(\epsilon)]\tilde{\varphi}_n(\epsilon,t)=1+\frac{u_n}{\pi}\int_{-\infty}^{\infty}d\epsilon_1\tilde{\varphi}_n(\epsilon_1,t)\frac{\mathrm{Im}\,G_A(\epsilon_1)}{\epsilon-\epsilon_1}\times[\theta(\epsilon_F-\epsilon_1)+\theta(\epsilon_1-\epsilon_F)e^{\iota(\epsilon-\epsilon_1)t}] \tag{9}$$

in terms of real and imaginary parts of the advanced Green's function,

$$\mathrm{Re}\,G_A(\epsilon)=\mathcal{P}\sum_i\frac{|c_{in}|^2}{\epsilon-\epsilon_i},\quad \mathrm{Im}\,G_A(\epsilon)=\pi\sum_i|c_{in}|^2\delta(\epsilon-\epsilon_i). \tag{10}$$

Making use of the expression for the density of states $\mathrm{Im}\,G_A(\epsilon)$ we obtain from Eq. (9)

$$\tilde{\varphi}_n(\epsilon,t)=\frac{1+u_n\Sigma_i\frac{|c_{in}|^2\varphi_i(t)}{\epsilon-\epsilon_i}[\theta(\epsilon_F-\epsilon_i)+\theta(\epsilon_i-\epsilon_F)e^{\iota(\epsilon-\epsilon_i)t}]}{1+u_n\,\mathrm{Re}\,G_n(\epsilon)}. \tag{11}$$

Clearly, to find $\tilde{\varphi}_n(\epsilon,t)$ the quantities

$$\varphi_i(t)\equiv\tilde{\varphi}_n(\epsilon_i,t) \tag{12}$$

must be known. However, to determine these functions we must know $\tilde{\varphi}_n(\epsilon_i,t)$. To escape this vicious circle, the finiteness of $\tilde{\varphi}_n(\epsilon,t)$ is used. One can show that, indeed, $\tilde{\varphi}_n(\epsilon,t)$ is finite for $t<\infty$ everywhere on the real axis, as well as when ϵ approaches the roots E_α^n of the equation

$$1+u_n\,\mathrm{Re}\,G_n(E_\alpha^n)=0. \tag{13}$$

Because of that $\tilde{\varphi}_n(\epsilon,t)$ is finite, and the nominator of the right-hand side of Eq. (11) must be equal to zero in these points:

$$1+u_n\sum_i\frac{|c_{in}|^2\varphi_i(t)}{E_\alpha^n-\epsilon_i}[\theta(\epsilon_F-\epsilon_i)+\theta(\epsilon_i-\epsilon_F)e^{\iota(E_\alpha^n-\epsilon_i)t}]=0,\quad \varphi_i(0)=1. \tag{14}$$

The solution of these algebraic time-dependent equations gives what we need: $\varphi_i(t)$. The inverse Fourier transform of $\varphi_n(\epsilon,t)$ (8), (11) yields finally

$$\varphi_n(\tau,t)=-\iota\sum_{i>F}\sum_\alpha|c_{in}|^2\varphi_i(t)\xi_{i\alpha}^n e^{-\iota E_\alpha^n\tau}e^{\iota(E_\alpha^n-\epsilon_i)t},\quad \tau>0. \tag{15}$$

The residues of the functions $\varphi(\epsilon,t)e^{-\iota\epsilon t}$ at $\epsilon=E_\alpha^n$ obey the useful sum rule[11]

$$\sum_\alpha\xi_{i\alpha}^n=1,\quad \xi_{i\alpha}^n=\frac{-1}{u_n(E_\alpha^n-\epsilon_i)\Sigma_j\left(\frac{|c_{jn}|}{E_\alpha^n-\epsilon_j}\right)^2}=u_n\frac{|\tilde{c}_{\alpha n}|^2}{\epsilon_i-E_\alpha^n}. \tag{16}$$

The reduction of the ND equation to the algebraic problem (11), (14), and (15) constitutes the main result of the present paper.

The zeros E_α^n of the denominator of $\tilde{\varphi}_n(\epsilon,t)$ (11) are nothing else than the spectrum of the ''completely relaxed'' valence shell due to a core hole in the nth atom. One can see that the eigenvalue problem (13) is equivalent to the standard secular problem associated with the equations

$$a_{\alpha i}^n(E_\alpha^n-\epsilon_i)+\sum_j V_{ij}^n a_{\alpha j}^n=0,\quad V_{ij}^n=u_n c_{in}^* c_{jn}. \tag{17}$$

The eigenvectors $\{a_{\alpha i}^n\}$ define the wave function of a valence electron in the field of a static core hole,

$$\tilde{\psi}_\alpha^n=\sum_i a_{\alpha i}^n\psi_i=\sum_n\tilde{c}_{\alpha n}\phi_n,\quad \tilde{c}_{\alpha n}=\sum_i a_{\alpha i}^n c_{in},$$

$$\sum_i |a^n_{i\alpha}|^2 = 1. \tag{18}$$

A. Limiting case: Fast and adiabatic XA

According to Eq. (3) the duration of x-ray absorption is restricted by the lifetime broadening. One can treat XA as a fast process when $u_n, \Delta\epsilon \ll \Gamma$. Here $\Delta\epsilon$ is the effective width of the valence band. In such a case the valence electrons have no time to rearrange in the field of the core hole ($u_n \to 0$): $E^n_i \simeq \epsilon_i - u_n |c_{in}|^2$, $\xi_{i\alpha} \simeq \delta_{\alpha i}$, $\varphi_i(t) \simeq 1$. Hence, the XA cross section is defined by the unperturbed propagators $\varphi_n(\tau,t) \simeq G_n(\tau)$, $g_n(t) \simeq ie^{iE_n t}$, and $K_n(\tau,t) \simeq ie^{iE_n t} G_n(\tau)$.

An adiabatic switching on of the core hole $[0,t] \Rightarrow [-\infty,\infty]$ forms the other extreme case. The system now has time to relax completely. The corresponding valence propagator (7) reads

$$\mathcal{G}_n(\epsilon) = \frac{G_n(\epsilon)}{1 + u_n G_n(\epsilon)} = \sum_\alpha |\tilde{c}_{\alpha n}|^2 \left\{ \frac{\theta(E^n_\alpha - \epsilon_F)}{\epsilon - E^n_\alpha + \iota 0} + \frac{\theta(\epsilon_F - E^n_\alpha)}{\epsilon - E^n_\alpha - \iota 0} \right\}. \tag{19}$$

The cross section for these two limits reads

$$\sigma^{f,\alpha}_n(\omega) = -2\pi\alpha\omega |d|^2 \, \mathrm{Im} \sum_n \begin{cases} G^-_n(\omega + E_n, \Gamma) & \text{fast,} \\ \mathcal{G}^-_n(\omega + E'_n, \Gamma) & \text{adiabatic.} \end{cases} \tag{20}$$

Here,

$$\mathcal{G}^-_n(\epsilon,\Gamma) = -2\iota\pi \sum_{\alpha > F} |\tilde{c}_{\alpha n}|^2 \Delta(\epsilon - E^n_\alpha, \Gamma),$$

$$E'_n = \tilde{E}'_n - u_n \sum_{\alpha > F} |\tilde{c}_{\alpha n}|^2, \tag{21}$$

and $\Delta(\epsilon,\Gamma) = \Gamma/\pi(\epsilon^2 + \Gamma^2)$. The lifetime-broadened unperturbed Green's function $G^-_n(\epsilon,\Gamma)$ is defined by the same expression (21) after replacements $\tilde{c}_{\alpha n} \to c_{in}$ and $E^n_\alpha \to \epsilon_i$.

B. Limiting case: Empty valence band

To understand the role of the band filling[17,7] we consider the XA profile of the completely empty valence band. Without valence electrons the creation of electron holes is impossible, and the final states are well-defined as strict Hartree-Fock states in the stationary field of the core hole. When the valence band is empty, Eq. (14), it is brought into the form

$$\sum_{i > F} \frac{|c_{in}|^2 \varphi_i(t)}{E^n_\alpha - \epsilon_i} e^{\iota(E^n_\alpha - \epsilon_i)t} = -\frac{1}{u_n}. \tag{22}$$

This and Eq. (16) show that the propagators (7), (15) coincide with the "completely relaxed" Green's functions,

$$\varphi_n(\tau,t) = \mathcal{G}^-_n(\tau) = -\iota \sum_{\alpha > F} |\tilde{c}_{\alpha n}|^2 e^{-\iota E^n_\alpha \tau},$$

$$g_n(t) = -i\theta(t) e^{\iota E'_n t}. \tag{23}$$

Thus, when the occupancy of the valence band decreases, the XA cross section becomes closer to the one in the adiabatic limit (complete relaxation).

IV. NONRESONANT X-RAY EMISSION

X-ray emission is an inverse process of x-ray absorption and the theory of the two processes follow similar steps. In contrast to XA, the initial state for XE is an ionic state $|n\rangle$ with a core hole (in the nth atom). The "relaxed" one-electron states ($\tilde{\psi}^n_\alpha, E^n_\alpha$) (17), (18) form the vacuum state $|n\rangle$. The golden-rule expression for the emission probability per unit time $\mathcal{P}(\omega')$ suggests the following time-dependent representation:

$$P_n(\omega') = \frac{(\alpha\omega')^3}{2\pi^2} \mathrm{Re} \int_0^\infty dt e^{-i(\iota\omega' + \Gamma)t} \langle n | \mathcal{D}^\dagger_n(t) \mathcal{D}_n(0) | n \rangle = \frac{(\alpha\omega')^3 |d|^2}{2\pi^2} \mathrm{Re} \int_0^\infty dt e^{-(\iota\omega' + \Gamma)t} K_n(t-0,t),$$

$$P(\omega') \equiv \frac{d\mathcal{P}(\omega')}{d\omega' d0'} = \sum_n P_n(\omega'). \tag{24}$$

Now the Hamiltonian reads $H = \Sigma_\alpha E^n_\alpha a^\dagger_\alpha a_\alpha + \mathcal{E}_n b^\dagger_n b_n + \Sigma_{\alpha\beta} u^n_{\alpha\beta} a^\dagger_\alpha a_\beta b^\dagger_n b_n$, where $u^n_{\alpha\beta} = u_n \tilde{c}^*_{\alpha n} \tilde{c}_{\beta n}$. The relation of $\mathcal{E}_n$ with the HF energy of the core electron will be clarified by Eq. (31) below. The two-electron propagator $K_n(\tau,t) = \Sigma_{\alpha\beta} \tilde{c}_{\alpha n} \tilde{c}^*_{\beta n} \langle n | T b_n(t) a^\dagger_\beta(\tau) a_\alpha(0) b^\dagger_n(0) | n \rangle$ factorizes similarly to photoabsorption (6): $K_n(\tau,t) = g_n(-t)\varphi_n(\tau,t)$. The Green's function of the valence electron $\varphi_n(\tau,t)$ satisfies the ND equation (7) after the replacements: $u_n \to -u_n$, $G_n(\tau) \to \mathcal{G}_n(-\tau)$, and $G_n(\tau - \tau_1) \to \mathcal{G}_n(\tau_1 - \tau)$. The propagator $\mathcal{G}_n(\tau)$ has the same expression as $G_n(\tau)$ (7) after replacement $(\epsilon_i, c_{in}) \to (E^n_\alpha, \tilde{c}_{\alpha n})$. The expression for the core-electron Green's function resembles (7)

$$g_n(-t) = -\iota\theta(t) \exp[-\iota\mathcal{E}_n t - \Delta(t)],$$

$$\Delta(t) = u_n \int_0^t d\tau \varphi_n(0_+, \tau). \tag{25}$$

The solution of the ND equation is similar to XA. The final result reads

$$\varphi_n(\tau,t) = \iota \sum_{\alpha < F} \sum_i |\tilde{c}_{\alpha n}|^2 \varphi_\alpha(t) \xi_{\alpha i} e^{\iota\epsilon_i \tau} e^{-\iota(\epsilon_i - E^n_\alpha)t}, \quad \tau > 0. \tag{26}$$

Here,

$$\xi_{\alpha i} = \frac{1}{u_n \Sigma_\beta |\tilde{c}_{\beta n}|^2 \frac{(\epsilon_i - E^n_\alpha)}{(\epsilon_i - E^n_\beta)^2}} = u_n \frac{|c_{in}|^2}{\epsilon_i - E^n_\alpha}, \quad \sum_i \xi_{\alpha i} = 1. \tag{27}$$

The functions $\varphi_\alpha(t)$ satisfy algebraic equations, which are similar to Eq. (14):

$$1-u_n\sum_\alpha \frac{|\tilde{c}_{\alpha n}|^2\varphi_\alpha(t)}{\epsilon_i-E^n_\alpha}[\theta(E^n_\alpha-\epsilon_F)+\theta(\epsilon_F-E^n_\alpha)e^{-\iota(\epsilon_i-E^n_\alpha)t}] =0, \quad \varphi_\alpha(0)=1. \tag{28}$$

A. Limiting cases

1. Fast and adiabatic XE

Analogously to XA (20) it is straightforward to write the formulas for the XE probability in the extreme limits,

$$P^{f,a}_n(\omega')=\frac{(\alpha\omega')^3|d|^2}{4\pi^2}\,\mathrm{Im}\sum_n \begin{cases} \mathcal{G}^+_n(\omega'+\mathcal{E}_n,\Gamma) & \text{fast} \\ G^+_n(\omega'+\mathcal{E}'_n,\Gamma) & \text{adiabatic.}\end{cases} \tag{29}$$

Here $\mathcal{E}'_n=\mathcal{E}_n+u_n\Sigma_{j<F}|c_{jn}|^2$,

$$\mathcal{G}^+_n(\epsilon,\Gamma)=2\iota\pi\sum_{\alpha<F}|\tilde{c}_{\alpha n}|^2\Delta(\epsilon-E^n_\alpha,\Gamma). \tag{30}$$

The same expression is valid for $G^+_n(\epsilon,\Gamma)$ after the following replacements: $\tilde{c}_{\alpha n}\to c_{in}$, $E^n_\alpha\to\epsilon_i$. To find $\mathcal{E}_n$ we first note that $(-E'_n)$ (21) in photoabsorption and that $(-\mathcal{E}'_n)$ means the ionization potential of the core level in the case of full relaxation of the core excited state. Clearly, they must be the same: $E'_n=\mathcal{E}'_n$. This yields

$$\mathcal{E}_n=E_n-u_n\sum_{j<F}|c_{jn}|^2+\delta_n,$$

$$\delta_n=u_n\left[\sum_{i>F}|c_{in}|^2-\sum_{\alpha>F}|\tilde{c}_{\alpha n}|^2\right]. \tag{31}$$

It is interesting to note that this formula differs from the expression for $\overline{E_n}$ (5).

2. Completely filled valence band

The role of band filling is clearly seen when the valence band is completely filled. This limit is inverse to the limit of empty valence bands in photoabsorption, but displays the same physics. The electron-hole pairs can then not be created since no unoccupied states are available. The only role of the annihilation of the core hole due to an emissive transition is to rearrange the relaxed valence states into unrelaxed ones. The calculations are very similar to the photoabsorption case. Making use of Eqs. (27) and (28) one can see that the propagators (26) and (25) coincide with the unrelaxed ones in this limit:

$$\varphi_n(\tau,t)=G^+_{nn}(-\tau)=\iota\sum_{i<F}|c_{in}|^2e^{\iota\epsilon_i\tau},$$

$$g_n(-t)=-\iota\theta(t)e^{-\iota E'_n t}. \tag{32}$$

The probability of x-ray emission is now given by the adiabatic limit (unrelaxed approximation) (29).

V. INNER-SHELL X-RAY PHOTOELECTRON SPECTRA

The next important process we consider is photoionization of a core electron. When the photon energy essentially exceeds the ionization potential of the core electron I_n, the cross section of the XPS process reads

$$\sigma(\varepsilon,\omega)=\sum_n \sigma_n(\varepsilon,\omega), \quad \sigma_n(\varepsilon,\omega) =4\pi\alpha\omega|d_{\mathbf{p}}|^2\,\mathrm{Im}\int_0^\infty dt e^{[\iota(\omega-\varepsilon)-\Gamma]t}g_n(t). \tag{33}$$

Here $d_{\mathbf{p}}=\int\psi^*_{\mathbf{p}}(\mathbf{e}\cdot\mathbf{r})1s_n d\mathbf{r}$ and $\psi_{\mathbf{p}}$ is the wave function of the photoelectron with momentum $\mathbf{p}$ and energy ε.

When the valence band is completely filled, the valence propagator (15) is equal to zero, $\varphi_n(\tau,t)=0$, and the Green's function coincides with the unperturbed one, $g_n(t)=-\iota\theta(t)\exp(\iota E_n t)$. This results in a single resonance for each atom (N resonances for the whole system) with the unperturbed ionization potentials I^0_n (34).

The case of an empty valence band was considered above; according to Eq. (23) the Green's function of a core electron coincides with the propagator in the limit of complete relaxation. In this case the photoelectron spectrum of each atom has a single resonance with the HF ionization potential (34).

The partial band filling ''opens'' the shake-up channels; the many-electron resonances appear on the high-energy side of the XPS spectrum. It is readily understood that the main one-electron resonance is shifted relative to the center of gravity $\langle\varepsilon\rangle_n$ into the low-energy side when the shake-up satellites appear. This is in accordance with the MA theorem,[14,15,8] which states that the center of gravity of the XPS spectrum of a core level

$$\langle\varepsilon\rangle_n=\omega-I^0_n, \quad I^0_n=-E_n \tag{34}$$

is equal to ''Koopman's value'' (see also below).

VI. EXCITONIC STATES

When the interaction strength exceeds the critical value u_{cr},

$$u_n>u_{\mathrm{cr}}=2|\beta|, \tag{35}$$

the lowest level is split off far from the main body of the valence spectrum of a core-hole state. For an insulator, such a local or excitonic level can appear also in the gap between occupied and empty states (this case is not considered here). The probability of shake-up transitions is enhanced strongly when the photon energy is sufficient to excite the second electron from the excitonic level. This leads to an additional high-energy band in the XA spectrum and in XPS.[18,17] The threshold of this band, $I_n+\Delta_{\mathrm{exc}}$, is shifted to the high-energy side relative to the main threshold I_n by Δ_{exc}, which is the energy of excitation from the excitonic level to the bottom of the unoccupied states. Clearly, the number of split levels is equal to the number of equivalent atoms because each atom has a particular relaxed spectrum.

The ''strict'' analysis shows that without a core hole the final state of the XE transition effectively lacks the signature of an excitonic state. One can only expect such a signature in a many-electron framework (shake-up transitions related to nonorthogonality of the one-electron orbital of initial and final states). The intensities of these transitions are weak and tend to zero with an increase in the size of the system. We note that the absence of the secondary threshold in XE from metals was predicted by Combescott and Noziéres.[17] The fast approximation (29) yields on the other hand a strong excitonic peak in XE, but this limit describes the real physics poorly.

VII. COMPUTATIONS

In the numerical simulations we study XA, XE, and XPS from the prototype systems containing linear chains of finite length. In particular we focus on the linear even polyenes with $N=2M$ atoms. The molecular orbital (MO) coefficients and MO energies of such a one-dimensional tight-binding model are given by Coulson formulas,

$$c_{in}=\left(\frac{2}{N+1}\right)^{1/2}\cdot\sin\left(\frac{in\pi}{N+1}\right),\quad \epsilon_i=\alpha+2\beta\cos\left(\frac{i\pi}{N+1}\right). \tag{36}$$

The parameter β defines the width of the valence band. We neglect the site dependence of E_n and the interaction strength u_n. The following parameters are used in the simulations: $\alpha=0$, $\beta=-2.4\,\mathrm{eV}$, and $\Gamma=0.09\,\mathrm{eV}$. We put the reference point of all energies in the middle of the unperturbed spectrum of the valence band by setting $\alpha=0$. The lifetime-broadened density of states (DOS) of the studied system is shown in Fig. 1. Let us restate that the lifetime-broadened DOS is obtained from the DOS (10) by the replacement $\delta(\epsilon-\epsilon_i)\to\Delta(\epsilon-\epsilon_i,\Gamma)$. To evaluate the XA cross section (3) we need the propagator $\varphi_n(t,t)$ (15). The sum rule (16) results in a very useful formula,

$$\varphi_n(t,t)=-\iota\sum_{i>F}|c_{in}|^2\varphi_i(t)e^{-\iota\epsilon_i t}, \tag{37}$$

which we implemented in the simulations. A similar result for the valence propagator (26) is straightforward.

We start the computations of XA and XPS by finding the ''relaxed'' one-electron states $(E^n_\alpha,\tilde{c}_{\alpha n})$ (17). The functions $\varphi_i(t)$ are computed for discrete times t as a solution of the time-dependent algebraic equation (14). At the next step we evaluate $\xi^n_{i\alpha}$ (16) and the propagators $\varphi_n(\tau,t)$ (15) for different times. After that the core-electron Green's function (7) is evaluated. The final step of the numerical procedure is the calculation of the correlator $K_n(t-0,t)$ (6) and the partial and full XA (3) and XPS (33) cross sections. To see the role of the electron-core-hole interaction, the XA cross section was also computed in the framework of the fast and adiabatic limits (20). The numerical procedure for XE is similar to XA.

We also implemented the direct numerical solution of the Dyson equation (7) using the discrete time grids as was done earlier in Ref. 5. This method requires much larger computational time and we used it only as a tool to check our main code.

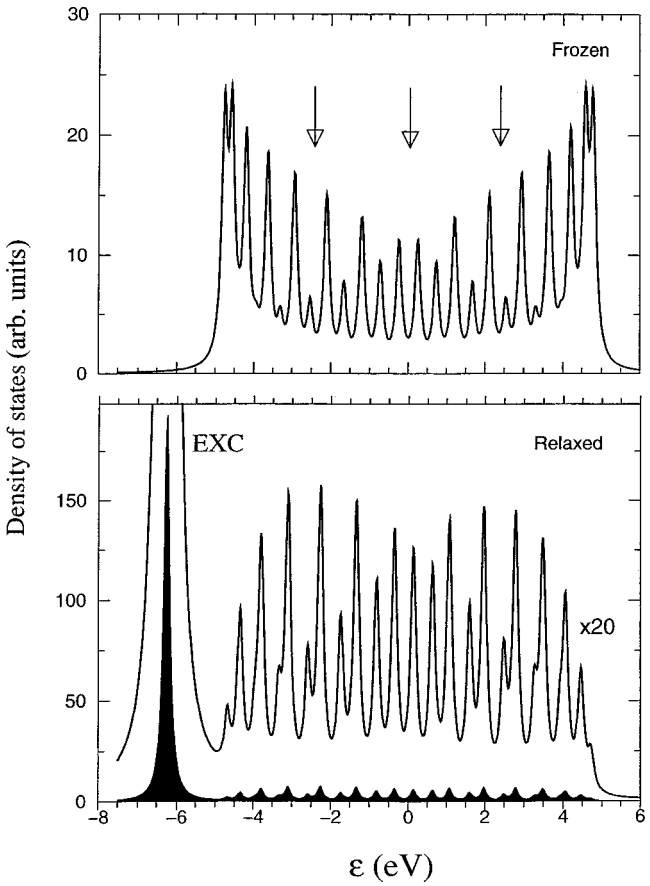

FIG. 1. The lifetime-broadened unperturbed and relaxed density of states $\mathrm{Im}\,G_A(\epsilon,\Gamma)$ (10) and $\mathrm{Im}\mathcal{G}_A(\epsilon,\Gamma)$ for the midatom $M=15$. $N=30$, $u_n=4\,\mathrm{eV}$, $\Gamma=0.09\,\mathrm{eV}$, and $\beta=-2.4\,\mathrm{eV}$. The strong low-energy peak in the lower panel corresponds to the excitonic state. The vertical arrows show the position of the Fermi level for different band fillings $\varrho=\frac{1}{3},0.5,\frac{2}{3}$.

VIII. RESULTS AND DISCUSSION

A. XA spectra

The interaction with the core hole may be activated in three ways: fast, adiabatic, and explicit, according to the evolutional ND equation. The XA spectral shapes in the fast and adiabatic limits copy the densities of unoccupied unrelaxed and relaxed states, respectively. These densities of states are the parts of the DOS lying above the Fermi level (Fig. 1). The comparison of strict calculations with the adiabatic (relaxed) approximation are shown in Figs. 2 and 3: The fast approximation leads to worse results, showing the inverse intensity distribution, Fig. 1. The photon frequency is given here relative to the core ionization potential of the midatom, which is $I_M=-E_M$ in the fast limit, while $I_M=-E'_M$ in the strict and the adiabatic calculations (20). The role of band filling (the ratio of the number of occupied states to all valence states),

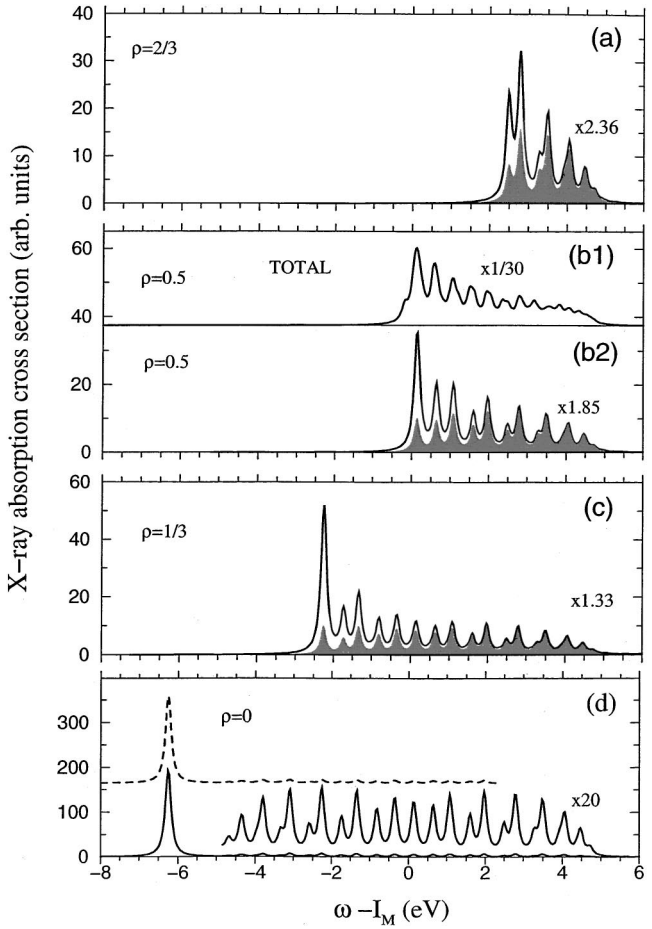

FIG. 2. The dependence of XA on band filling ϱ (38). (a), (b2), (c), and (d) show the partial XA cross section of the bulk (Mth) atom, while (b1) shows the total XA cross section from all N atoms (decreased by 30 times). The solid line: strict solution; the shaded profiles and dashed line: adiabatic approximation. The numbers $k=2.36$, 1.85, and 1.33 denote that the corresponding adiabatic cross section is enlarged by k times. $N=30$; $u_n=4$ eV.

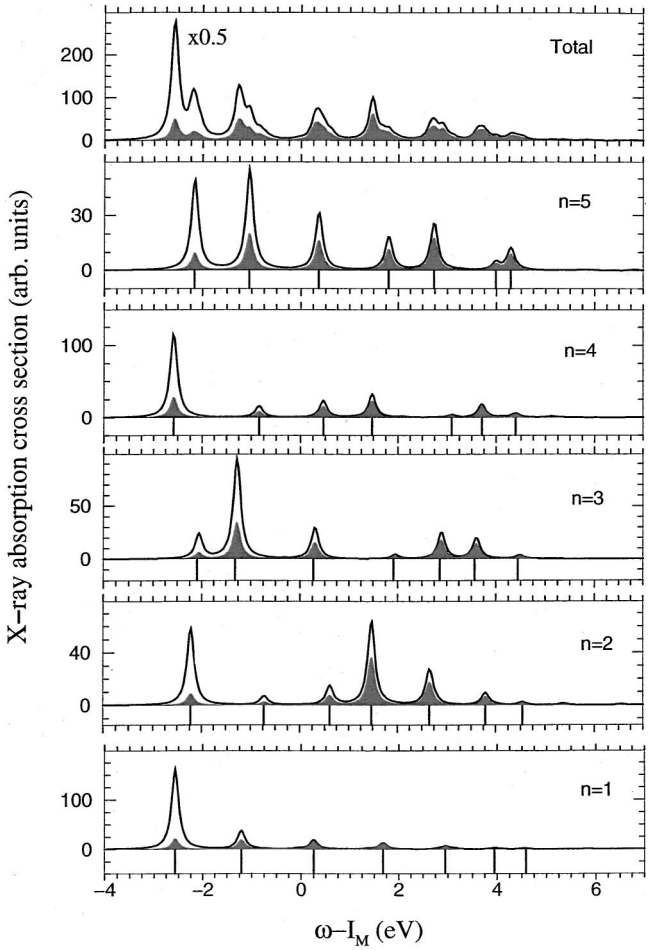

FIG. 3. The site dependence of XA spectra: exact results versus adiabatic approximation. Panels with $n=1,..,5$ present adiabatic (filled profiles) and strict (solid lines) partial XA cross sections. The total cross sections (upper panel) are decreased by 2 times. The bars show the relaxed spectrum $\{E_\alpha^n\}$ (13). $N=10$, $\varrho=0.3$, and $u_n=4$ eV.

$$\varrho=\frac{N_{\rm occ}}{N},\quad 0\leqslant\varrho\leqslant 1, \tag{38}$$

can be seen from Fig. 2. The adiabatic approximation differs from the strict calculation mainly in the region adjoint to the XA edge where the Mahan-Noziéres-De Dominicis (MND) singularity begins to form. One can see the expansion of the region of coincidence of the discussed spectral profiles towards the XA edge with a decrease of the band filling ϱ. Both spectral profiles coincide exactly for an empty band $\varrho=0$ (Sec. III B). Since the excitonic level is now empty, it becomes active in XA and gives a dominant contribution because of $u_n\sim u_{\rm cr}$ (Fig. 2). The comparison of Figs. 1(b1) and 1(b2) indicates that the spectrum of a bulk atom reproduces the main spectral features of the total XA cross section of the chain with $N=30$.

Let us now turn attention to the site dependence of the XA spectra of the moderate size chain with $N=10$ (Fig. 3). Both strict and adiabatic approaches demonstrate strong site dependence of the XA profile, referring both to intensities and relaxation energies $\{E_\alpha^n\}$ (Fig. 3). Similar to Fig. 2, one can observe a better agreement between the strict and adiabatic approaches in the high-energy region of the spectra. Contrary to the partial cross sections, the total cross section is enhanced close the XA edge where the MND singularity forms. Apparently, the total XA spectrum is close to the XA spectral shape of the midatom for the long chains where the site dependence is negligible.

Both Figs. 2 and 3 show that the adiabatic approximation (20) gives a smaller area of the XA profile, $\sigma_n^a=\int\sigma_n^a(\omega)d\omega=4\pi^2\alpha\omega|d|^2\Sigma_{\alpha>F}|\tilde{c}_{\alpha n}|^2$, than the strict approach $\sigma_n=\int\sigma_n(\omega)d\omega$. A reason for this can be found in the following sum rule:

$$\sigma_n=\sigma_n^f=4\pi^2\alpha\omega|d|^2\sum_{i>F}|c_{in}|^2>\sigma_n^a, \tag{39}$$

which states that σ_n coincides with the fast limit value[6] σ_n^f. The adiabatic cross section is suppressed, $\sigma_n^a<\sigma_n$, since the excitonic state borrows the main part of the relaxed density of states $\mathrm{Im}\,\mathcal{G}_A(\epsilon)$ (Fig. 1).

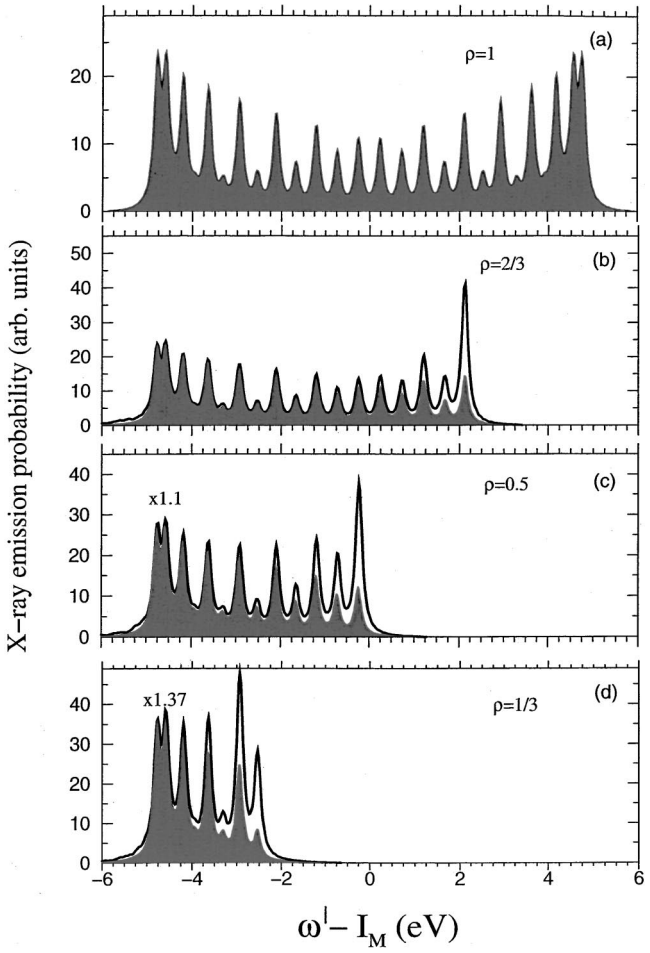

FIG. 4. The dependence of XE from the bulk atom on the band filling ϱ (38). The shaded profiles and solid lines present the results of the adiabatic approximation and strict approach, respectively. The shaded profiles in (c) and (d) are enlarged by 1.1 and 1.37 times, respectively. $N=30$; $u_n=4$ eV.

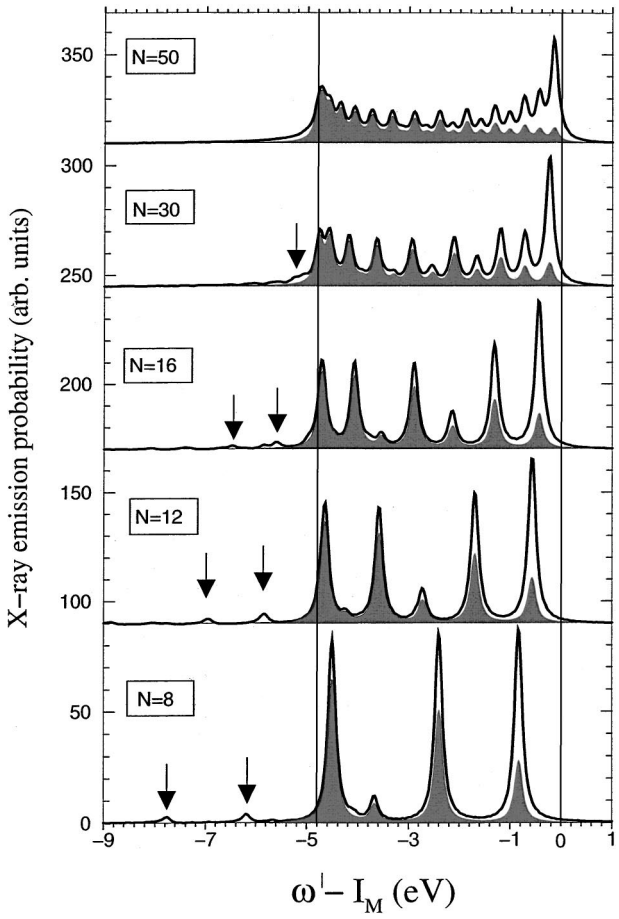

FIG. 5. The dependence of XE spectra and shake-up contributions on the chain length for the bulk atom ($n=M$). $N=50$, 30, 16, 12, and 8. Solid line: strict time-dependent calculation; shaded profiles: adiabatic approximation (29). The arrows indicate position of shake-up resonances. Vertical lines show the margins of the occupied valence band $[-4.8; 0]$ eV. $\varrho=0.5$; $u_n=8$ eV.

B. XE spectra

Opposite to XA, x-ray emission in the fast and adiabatic approximations (29) copies the densities of occupied states, which are, respectively, the parts of the relaxed and unrelaxed DOS below the Fermi level (Fig. 1). We first analyze the role of the band filling (Fig. 4). To be specific we treat the midatom and consider the frequency of the emitted photon relative to the core ionization potential of the midatom; this is $I_M=-\mathcal{E}_M$ in the fast limit, while $I_M=-E'_M=-\mathcal{E}'_M$ in the strict and adiabatic calculations (29). A consideration of the fast limit case (Fig. 1) shows that this limit is too crude for XE: In contrast to the case of fast absorption, neither the strict approach nor the adiabatic limit shows excitonic resonances (see Sec. VI). Similar to photoabsorption the adiabatic approximation agrees with the strict calculation, except for the region close to the Fermi level, where one can see the trend of a formation of a MND singularity. The agreement improves essentially with growth of the band filling. When the band is completely filled the adiabatic approximation (the unperturbed density of states) coincides exactly with the strict solution (see Sec. IV A 2).

The dependence of XE spectra and shake-up transition intensities on the length of the system is illustrated by Fig. 5. When the chain is short, we see clearly weak shake-up resonances below the main body of the XE band. The first shake-up resonance occurs due to transitions of the electron from the highest occupied MO (HOMO) to the lowest unoccupied MO (LUMO). The amplitude of shake-up resonances decreases with the increase of length of the system. The distance between shake-up resonances decreases with the increase of the system length due to an increase of the density of states. The shake-up resonances move towards the bottom of the occupied band due to a decrease of the gap between HOMO and LUMO with an increase of N. They form the low-energy tail in the XE spectra of long chains. The formation of the ''double peak'' shape of XE is clearly seen for large N. The low-energy peak is due to the unrelaxed density of states (Fig. 1), while the stronger high-energy peak shows the formation of the MND singularity.

Similar to XA, the area of the XE profile, $P_n^a=\int P_n^a(\omega')d\omega'=[(\alpha\omega')^3|d|^2/2\pi]\Sigma_{i<F}|c_{in}|^2$, in the adiabatic approximation (29) is smaller than in the strict approxi-

mation $P_n = \int P_n(\omega')d\omega'$ (see Figs. 4 and 5). To understand this we consider the sum rule,

$$P_n = P_n^f = \frac{(\alpha\omega')^3|d|^2}{2\pi}\sum_{\alpha<F}|\tilde{c}_{\alpha n}|^2 > P_n^a, \qquad (40)$$

which says that P_n coincides with the fast limit value[6] P_n^f. Hence, the reason for $P_n > P_n^a$ is the enhancement of P_n due to a large excitonic contribution in the sum over α in Eq. (40) (see Fig. 1).

C. The final-state rule for XA and XE

The analysis of XA and XE above shows that the relaxed solution describes the XA profile well while the frozen orbital approximation is more appropriate for the analysis of XE data. Indeed, the relative resonant energies of XA and XE one-electron transitions are equal to the adiabatic values $\omega(1s_n \to \psi_j) - I_n \simeq E_j^n$, $\omega(\psi_i \to 1s_n) - I_n = -I_i \simeq \epsilon_i$, respectively. Here I_i is the ionization potential of the valence level. However, it is clear that such an agreement for the spectral profile is not complete, for example, because of the MND edge singularities von Barth and Grossmann formulated the so-called final-state rule (FSR).[12] The intensity distribution is a product of the adiabatic and the ND profiles (see also Refs. 19 and 8). This rule adapted for the discrete spectrum reads

$$\sigma_n(\omega) = \sigma_n^a(\omega)\Lambda_n(\omega), \quad P_n(\omega') = P_n^a(\omega')\Lambda_n(\omega'),$$
$$\Lambda_n(\omega) = \kappa\left(\frac{\epsilon_i^2}{(\omega-\epsilon_i-I_n)^2+\Gamma^2}\right)^{\alpha_n/2}, \quad \alpha_n = 2\frac{\delta_n}{\pi} - \left(\frac{\delta_n}{\pi}\right)^2. \qquad (41)$$

The parameter κ is here defined from the best fit to the strict solution. The phase shift due to scattering of the valence electron on the core hole can be calculated using the Friedel formula.[20,17]

$$\delta_n = \pi\left(\frac{\epsilon_i - E_i^n}{\epsilon_{i+1} - \epsilon_i}\right). \qquad (42)$$

The ND theory operates with the phase shift at the Fermi surface. We encounter some uncertainty concerning the value of ϵ_i in Eqs. (41) and (42), and the best agreement with the exact solution for XE is received when ϵ_i is equal to the energy of the highest occupied valence level ϵ_F. In the XA case the best agreement is obtained when ϵ_i coincides with the energy of the lowest unoccupied valence level. The FSR expressions coincide with the adiabatic limits $\sigma_n^a(\omega)$ and $P_n^a(\omega')$ when the interaction with the core hole is weak, $\delta_n \ll \pi$.

Figure 6 shows the photoabsorption by the bulk atom. The intensities as well as the transition energies in the fast (unrelaxed) limit differ strongly from the strict values. The transition energies in the adiabatic (relaxed) approximation coincide exactly with the strict calculation. One can see a certain improvement also in the intensity distribution, except at the edge where the MND singularity forms. The FSR correction of the adiabatic approximation changes the picture drastically: We now see quantitative agreement with an exact calculation. When we implement FSR for XE (see Fig. 7) we obtain an even worse agreement between the fast approximation and the strict result. A salient disagreement concerns the region for the strong excitonic peak given by the fast approximation (see Sec. VI) where the strict result only shows very weak two-electron satellites. The adiabatic approximation reproduces exactly the transition frequencies, however, the intensity distribution differs essentially from the exact spectrum. FSR improves the adiabatic approximation up to almost complete coincidence with the strict calculation. It is necessary to point out that the FSR correction increases the emission intensity near the top of the occupied band where the MND singularity appears. We note that the discussed trends are typical for all atoms and different lengths of the chain.

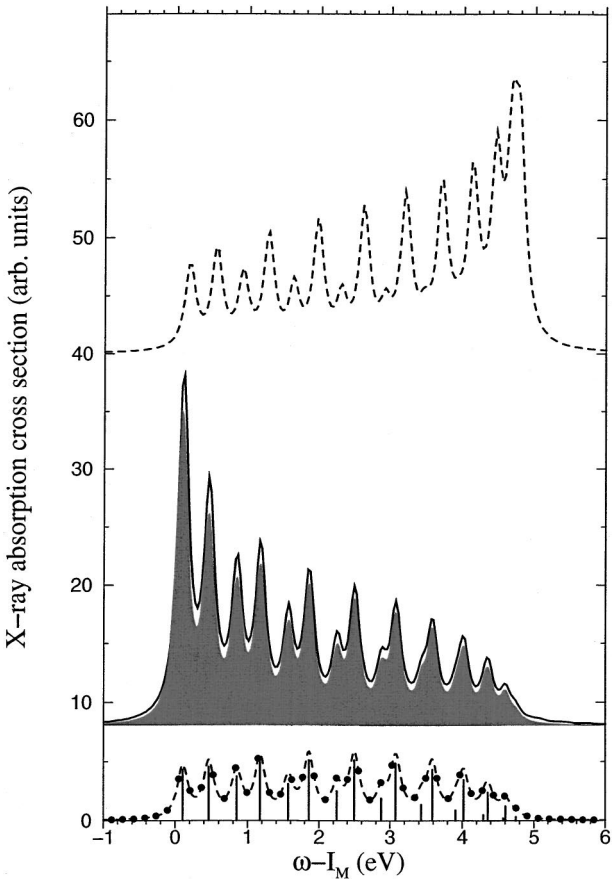

FIG. 6. The final-state rule in x-ray absorption by the bulk (Mth) atom. Dashed line: fast approximation (20), dashed line with filled circles: adiabatic approximation (20), solid line: strict solution, and shaded profile: final-state rule (41). The shaded profile is enlarged by 5.7 times. $N=40$, $\varrho=0.5$, and $u_n=4$ eV.

D. XPS spectra

The XPS profile of the nth atom consists of only a single resonance $\omega - \varepsilon = I_n^0$, if the interaction with the core hole u_n is neglected. To be specific we discuss here the spectra of the Mth bulk atom. With an increase of u_n the shake-up transitions begin to form the high-energy tail of a main peak, Fig. 8. As soon as u_n approaches $u_{cr} = 4.8$ eV (35), the shake-up

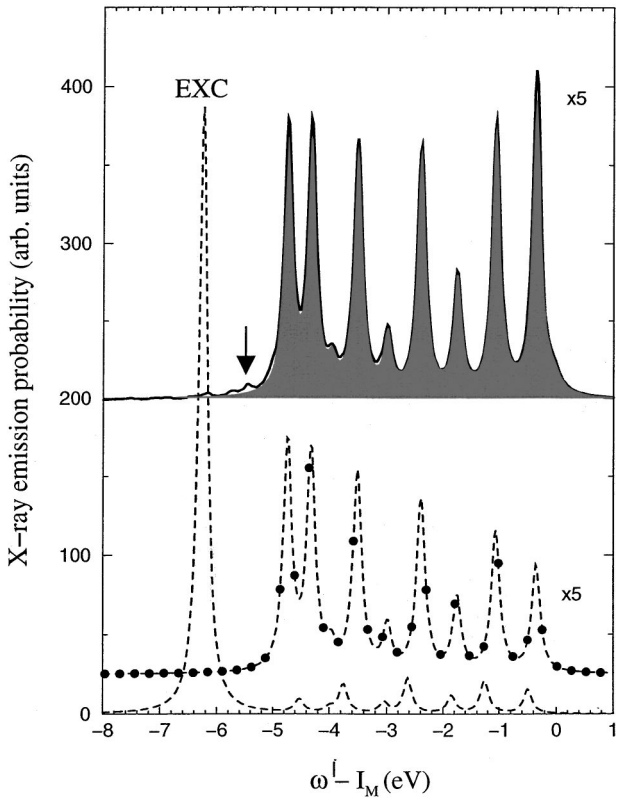

FIG. 7. The final-state rule in x-ray emission by the bulk (Mth) atom. Dashed line: fast approximation (29), dashed line with filled circles: adiabatic approximation (29), solid line: strict solution, and shaded profile: final-state rule (41). The arrow marks the shake-up band. The excitonic peak in the fast XE spectrum is marked by ''EXC.'' The FSR, strict, and adiabatic profiles are enlarged by 15, 5, and 5 times, respectively. The other input data are the same as in Fig. 6, except $N=20$.

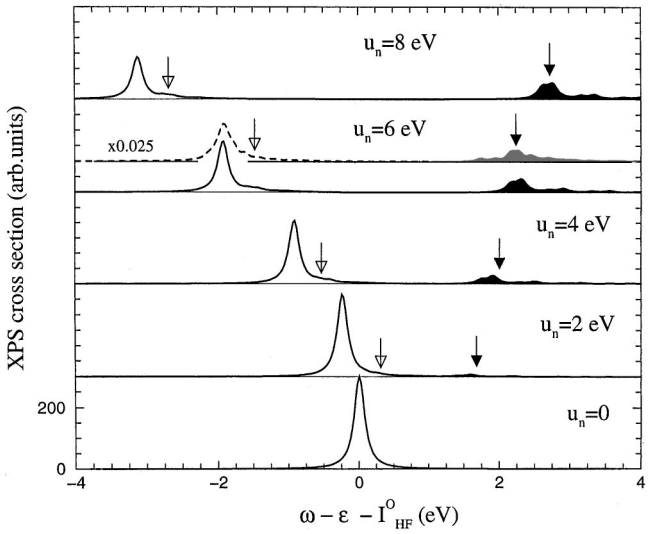

FIG. 8. The XPS profile (33) of the bulk atom (Mth atom) for different strengths of interaction with the core hole u_n. $N=40$, $\varrho=0.225$. The full XPS spectrum (summed over all atoms and divided by N) is shown by a dashed line. The filled and hollow arrows mark shake-up transitions from excitonic (filled profiles) and from HOMO to LUMO, respectively. The centers of gravity of the spectra coincide exactly with $\omega-\epsilon=I_n^0$ (34).

channels involving the excitonic level are opened. The gap between the main and excitonic thresholds becomes larger with an increase of u_n because of the lowering of the exciton energy. The site dependence of I_n leads to a broadening of the spectra. This effect though can be neglected for long chains. The comparison of the whole spectrum (dashed line) with a spectrum of bulk atoms (solid line) of a long chain confirms this, Fig. 8.

We consider now the spectra of bulk atoms when the interaction with the core hole is sufficient to split the local level from the main body of the occupied band (Fig. 9). We see clearly two qualitatively different groups of shake-up transitions related with the main and excitonic channels. The threshold of the shake-up transitions of the main channels is equal to the excitation energy from the HOMO to the LUMO. The transition energies are the differences of the corresponding energies E_α^n of the ''relaxed'' spectrum. The shake-up transition from the excitonic level to LUMO starts the second shake-up band. Apparently, the threshold of the excitonic band (energy distance from main resonance) $\Delta_{\rm exc}=E^n_{\rm LUMO}-E^n_{\rm exc}\simeq\epsilon_F-E^n_{\rm exc}$ increases linearly when the Fermi energy [and the band filling ϱ (38)] increases. When the band is completely filled we see only a one-electron resonance (Sec. V). The intensity of the excitonic band increases with the decrease of the band filling up to $\varrho\to0$. When $\varrho\to0$, the excitonic threshold takes a minimum value equal to the distance of the local level from the bottom of the main valence band. Again, only one-electron resonances form the XPS spectrum when the band, as well as the excitonic state, is empty. Such a discontinuous dependence of the excitonic band intensity on the band filling ϱ is due to a special shape of the density of states, Fig. 1, which takes a maximum value at the bottom and at the top of the valence band. It should be mentioned that the intensity of the excitonic band peaks near $\varrho\sim0.5$ if the unperturbed density of state has a belllike shape,[7] which is opposite to that used here (Fig. 1).

Both Figs. 8 and 9 show that the shake-up band reduces the intensity of the main one-electron resonance. The reason for this is the constant value of the area of the XPS profile (33): $\int\sigma_n(\varepsilon,\omega)d\varepsilon=4\pi^2\alpha\omega|d_{\mathbf{p}}|^2$. The center of gravity of XPS coincides exactly with the HF value (34) in accordance with the MÅ theorem[14,15] (Figs. 8 and 9): The main one-electron peak is pushed out into the low-energy side when many-electron satellites appear on the high-energy side (a ''lever arm'' relationship). A deep analysis of this theorem has been given by Almbladh and Hedin.[8] One should note that the often used treatment of $\overline{E_n}$ in the Hamiltonian (5) as E_n leads to wrong shifts of the XPS bands, and results in a violation of the center-of-gravity theorem.

E. Dynamics of the readjustment of valence electrons in the field of a transient core hole

1. The time dependence of propagators

The dynamical aspect of the interaction with a core hole is the heart of the studied problem. The natural way to under-

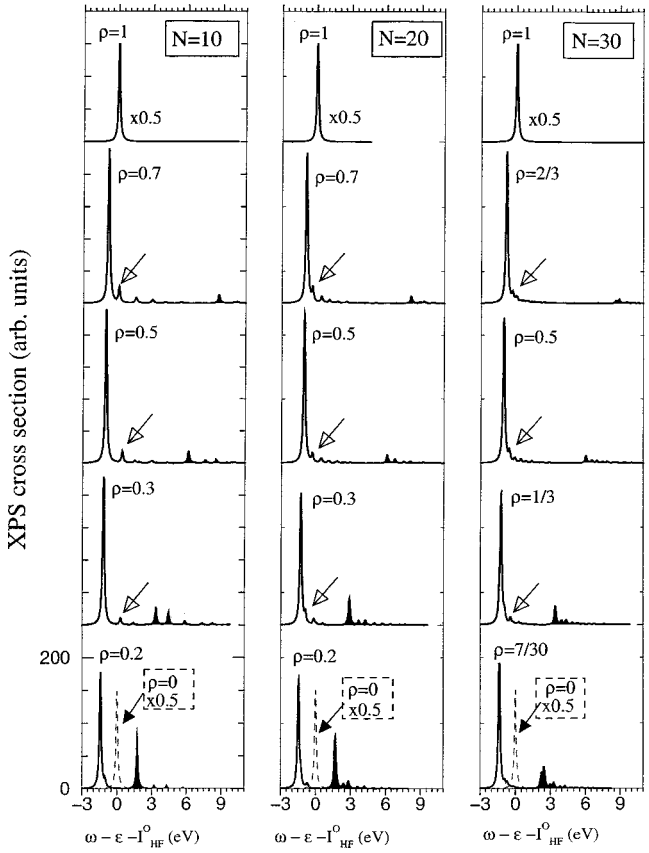

FIG. 9. The XPS profile (33) of the bulk atom (Mth atom) for different band fillings ϱ (38) and different chain lengths N. $u_n = 5\ \mathrm{eV} > u_{cr} = 4.8\ \mathrm{eV}$ (35). The hollow arrows show the shake-up transitions from HOMO to LUMO. The shaded profiles correspond to the shake-up transitions from the excitonic level. The position of the centers of gravity of spectra is $\omega - \epsilon = I_n^0$ (34).

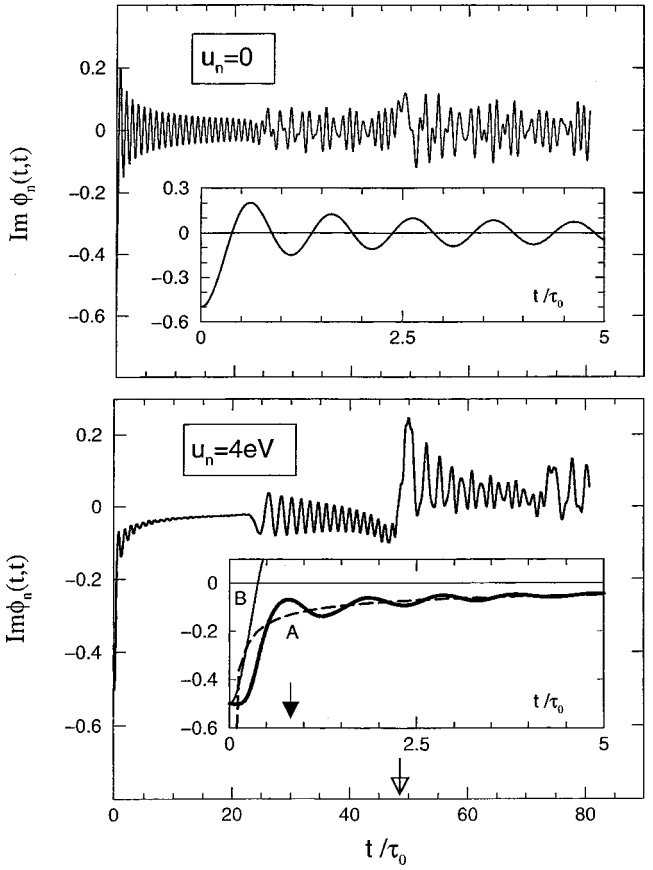

FIG. 10. The imaginary part of the valence electron propagator $\varphi_n(t,t)$ (37) of the midatom. $N=150$, $\varrho=0.5$. The upper panel displays the imaginary part of the free-electron Green's function $\mathrm{Im}\, G_n(t)$. The filled and hollow arrows mark the positions of the "relaxation" time τ_0 and revival time τ_R (43), respectively. The following notations are used in the inset of the lower panel. The dashed line A shows the ND asymptote (44) with the phase (42) $\delta_n \simeq 0.7$. The thin solid line B is the $\mathrm{Im}\, G_n(t)$ from the upper panel. The thick solid line is the strict solution.

stand the dynamics is to analyze the time evolution of the valence and core-electrons propagators. Two characteristic time scales are responsible for the dynamics:

$$\tau_0 = \frac{2\pi}{\Delta_u}, \quad \tau_R = \frac{2\pi}{\nu} = \tau_0 M. \tag{43}$$

The shortest time scale τ_0, describing fast oscillations, is related to the inverse bandwidth of the unoccupied band Δ_u (in our case $\Delta_u = 2|\beta|$ and $\tau_0 \simeq 0.9\ \mathrm{fs}$). The density of states or distance between valence levels $\nu = \Delta_u / M$ gives the second characteristic time scale $\tau_R \simeq 0.9\ \mathrm{M\,fs}$. Approximate positions of these time scales τ_0 and τ_R are shown in Figs. 10 and 11. These times are related with three essentially different dynamical regions. According to Fig. 10 the first step of relaxation, $0 < t < \tau_0$, is described approximately by $G_n(t)$. One can ask what happened during τ_0. It is possible to say that the valence shell relaxed partially during this time. The motivation for this is seen directly from Fig. 10 showing the relaxation suppression of the oscillations of $\varphi_n(t,t)$ compared with $G_n(t)$.

The MND spectral profile begins to form during the next time lapse $\tau_0 < t < \tau_R$, with the XA intensity being redistributed towards the edge. Figure 10 demonstrates that the ND asymptotic solution,[4]

$$\varphi_n(t,t) \approx C \left(\frac{\tau_0}{t} \right)^{1 - 2\delta_n/\pi}, \quad \tau_R > t \gg \tau_0 \tag{44}$$

almost coincides with the strict solution in this time domain except for the oscillations. These damping oscillations of the strict solution relative to the ND asymptote are though small when u_n is comparable with the bandwidth. The amplitude of these oscillations is suppressed compared with the unperturbed Green's function $G_n(t)$ due to the "charge transfer" into the excitonic state (Fig. 1).

One can see that the Green's functions (Fig. 10) and $\mathrm{Re}\, \Delta_n(t)$ (Fig. 11) almost recover their fast oscillations after the "revival" time τ_R (strictly speaking we have a set of the revival times). The display of the fine structure of the molecular spectrum including the sharpening of the MND edge singularity begins during the third step of the evolution: $t > \tau_R$. We discover here that for finite-size systems there is a

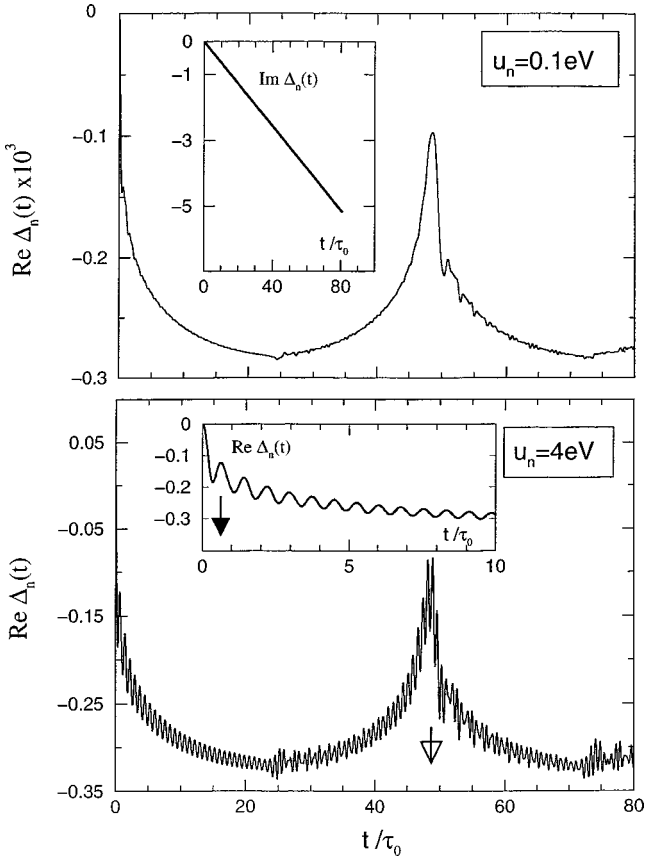

FIG. 11. The exponent $\Delta_n(t)$ of the core-electron Green's function of the midatom (7). Other notations are the same as in Fig. 10.

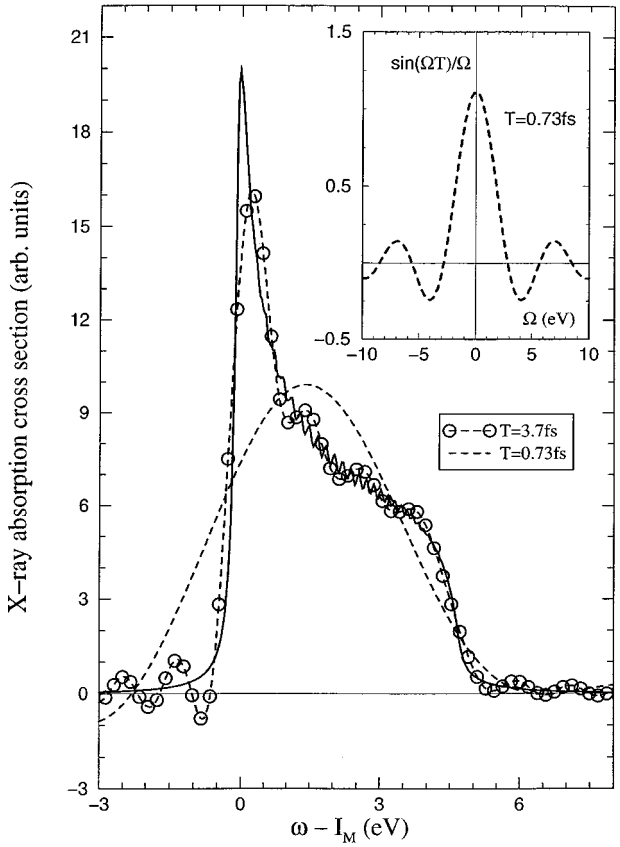

FIG. 12. Formation of the XA spectrum of the bulk atom as a function of time T. $N=150$, $u_n=4$ eV, and $\varrho=0.5$. Solid line: $T=\infty$.

breakdown of the ND asymptote for large times, $t>\tau_R$ (Fig. 10). The revival time (43) tends to infinity when the size of the system increases ($N\to\infty$) and the spacings between valence levels disappear. This is the case of metals with a continuous spectrum. Clearly, to see the fine structure, the lifetime and the measurement time must exceed the revival time, $t>\tau_R$ (see also the next section). It is interesting here to observe that the time lapse (44) for the validity of the ND asymptote becomes smaller when the size of the system decreases. Moreover, the ND scenario has no time to develop for small molecules $N<10$, where $\tau_0\sim\tau_R$.

2. Time evolution of XA, XE, and XPS profiles

We consider now an experiment with a finite time delay T, between the instant measurement and the beginning of interaction with the x-ray light. The corresponding observables, $\sigma_n(\omega|T)$, $P_n(\omega'|T)$, and $\sigma(\varepsilon,\omega|T)$ are defined by Eqs. (3), (24), and (33), respectively, after replacing the upper limits in the time integrations: $\infty\to T$. The results of the corresponding evaluations for different times T are displayed in Figs. 12, 13, and 14. The short-time picture ($T\ll 1/\Gamma$) is approximately the same for all spectra. We thus see a broad spectral profile with small sign-changing tails. The origin of such a signal can be understood from the expression for the imaginary part of the polarization describing the interaction of light with two levels, n and 0,

$$\mathrm{Im}\,\mathcal{P}\sim\frac{\sin(\omega-\omega_{n0})T}{\omega-\omega_{n0}},\quad \Delta\omega\lesssim\frac{1}{T}. \tag{45}$$

This expression implies that the interaction of radiation with a target forms a periodical sequence of absorption and emission for times shorter than the lifetime.[21,22] Let us note that the averaging of the signal over the finite time of a measurement removes the negative contributions.[22] What we learn from Eq. (45) is nothing but the uncertainty relation: The spectral resolution cannot be better than the inverse delay time $1/T$. Figures 12, 13, and 14 demonstrate that the formation of narrower spectral features requires more time. This is seen more clearly from snapshots of the XA spectra of a long chain, Fig. 12. Here we first observe the formation of a smooth high-energy part of the spectrum and then the slower formation of the sharp MND singularity. XE deserves a special comment in this context. Contrary to intuition in XE we do not see any excitonic peak even for very short times. This can be referred to the fact that the characteristic time of the readjustment of the relaxed one-electron states due to the switching off of the core-hole potential is the inverse bandwidth of the relaxed spectrum $1/\Delta E^n_\alpha$, and that one can expect to observe excitonic states only for $T<1/\Delta E^n_\alpha$. However, the energy resolution $\sim 1/T$ anyway does not allow this in principle.

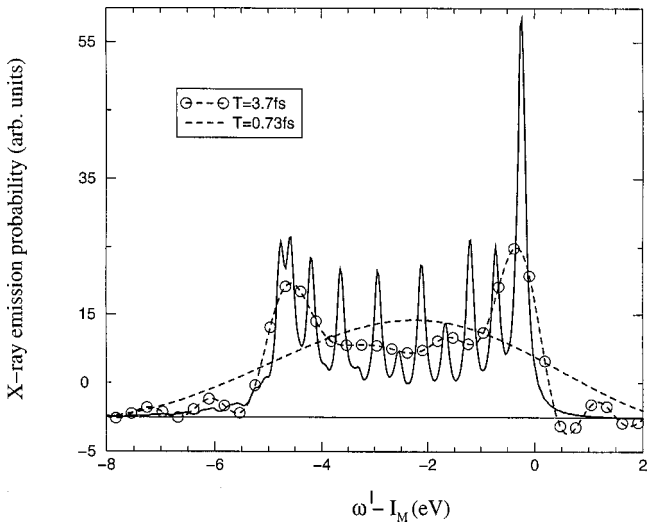

FIG. 13. Formation of the XE probability of the bulk atom as a function of time T. $N=30$, $u_n=8$ eV, and $\varrho=0.5$. Solid line: $T=\infty$.

IX. SUMMARY

Time-dependent formalisms appeal to our inclination to relate observations to processes which progress in time. In the area of x-ray spectroscopy and x-ray scattering such formalisms have proven to be very successful in predicting and analyzing phenomena associated to the coupling of nuclear motion.[2] A goal has been to achieve an analogous formalism for the electronic degrees of freedom in the formation of x-ray spectra. Such a formalism could, for example, aid in exploring and understanding the role of relaxation in x-ray spectroscopies, which is of fundamental importance for their applicability in molecular and material science.

To our knowledge only the theory of Noziéres and De Dominicis (ND) (Ref. 4) has addressed a rigorous time-dependent treatment of core-hole effects in x-ray spectra. For infinite-size systems like metals, the ND equation admits a strict solution only in the limit of large time lapses.[4] We explore in this paper the formation of x-ray spectra in the general cases of finite-size systems and provide strict solutions of the ND equation in the whole time domain. Our approach is based on the reduction of the ND integral equation to linear time-dependent algebraic equations. We apply our technique also to infinite-size systems through extensions of the system size.

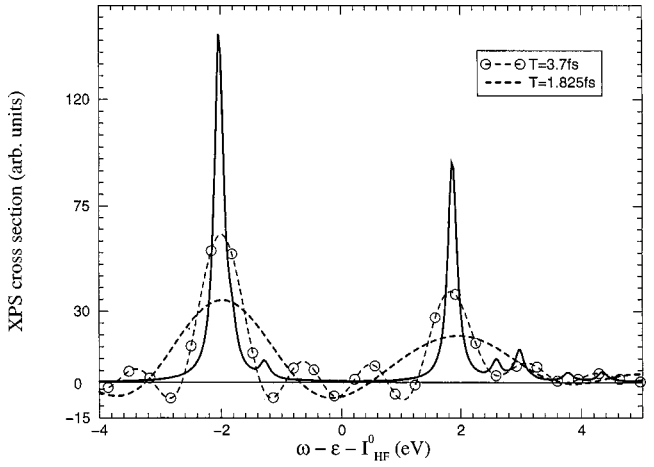

FIG. 14. Formation of XPS of the bulk atom as a function of time T. $N=20$, $u_n=6$, and $\varrho=0.2$. Solid line: $T=\infty$.

Clearly, the long-time ND asymptote cannot describe the whole spectral region, especially not so for finite systems. To understand the nature of the electronic readjustment due to a molecular core hole we explore the evolution of the valence and core-electron propagators as well as the full x-ray spectra on the real time scale. The present study of the electronic dynamics in the whole time domain demonstrates a richer dynamics for molecules compared to solids. Two characteristic time scales responsible for the relaxation dynamics were found, namely, fast oscillations related to the inverse bandwidth of the unoccupied band, and slow oscillations or revivals related to the inverse distance between the adjacent valence levels. These time scales are related with three essentially different dynamical regions, with, respectively, valence relaxation, formation of the MND profile, and formation of a molecular spectrum and a sharpening of the MND profile near the edge. These dynamical regions are of course very dependent on size and character of the system, and on the organization of the energy bands. The revival time must be smaller than the lifetime and the measurement time to produce a fine structure in the spectrum. We found that the long-time ND asymptote ceases to be valid when the time exceeds the revival time, which is proportional to the system size. For small molecules this means that there is simply no time for the MND singularity to develop. On the other hand, when the size of the system increases and the spacings between valence levels disappear, as in the case of metals, the revival time tends to infinity and there will be a sharp MND singularity.

To estimate the dynamics of the formation of the x-ray spectra, the XE, XA, and XPS profiles were simulated for different times of interaction with the radiation. It was found that short-time interaction leads to broad spectral profiles, which though is nothing but a manifestation of the uncertainty relation. When the time increases, one can observe a development of a fine structure and the MND singularity in XA and XE. The excitonic level, split from the bottom of the occupied valence band, appears only in the core excited state. One can expect to observe this level in XE only at the very beginning of the emission process. However, in practice this is impossible due to the large broadening of the spectrum for short times. The shake-up band related with the excitonic level is seen clearly in XPS. The manifestation of such a second threshold in XA (Ref. 17) is weaker.

The comparison with the strict solution of the ND equation shows that the adiabatic approximation describes XA and XE essentially better than the fast approximation. This explains the suppression of the relaxation effects in XE of gas phase and surface adsorbed molecules. However, our numerical simulations show a quantitative distinction between the adiabatic approximation and the strict approach. This distinction becomes significant for longer chains. To take the nonadiabaticity of the of x-ray transitions into account we

adapted the finite state rule[12] to molecules and found an almost complete numerical agreement between this rule and the strict XA and XE profiles for chains of different lengths. The simulations indicate that the final-state rule correction is important mainly near the XA edge and at the top of the XE band.

Special attention was paid to the size of the system. XA and XE spectra clearly show site dependency, which becomes negligible for an infinite chain, where the bulk atom contributions dominate. These spectra show a sharpening of a threshold MND singularity with the increase of the system size. We found an enhancement of the strength of the excitonic band in XPS with a decrease of the size of system and with the decrease of the band filling. The investigation of the role of band filling in molecular x-ray spectra shows a close resemblance with the corresponding trend in solids, namely, the suppression of many-electron effects towards an empty or a completely filled valence band.

The computational applications outlined in this work should very well be extendable to a more precise *ab initio* electronic structure framework. In that connection it is relevant to qualify the limitations of the MND model itself. This model operates with noninteracting quasiparticles in the valence shell and, hence, neglects collective excitations, for example, plasmon excitations in metals giving rise to sidebands. This is probably still not of any large consequence for finite systems. However, the multiplet structure caused by configurational interaction and exchange interaction with inner-shell spin can certainly be important and should be accounted for in systems like transition metals. Another effect lying beyond the standard MND model is the dynamical screening of the core-hole potential resulting in the reduction of the interaction of the valence electrons with the core hole. The role of this effect is a dependence of the scattering phase on the excitation frequency. These and other aspects of the limitations of the MND model were reviewed in Refs. 8 and 10. Notwithstanding these limitations we believe that an application of the MND model generalized in the way outlined in this work can have wide ramifications for the understanding of the formation of x-ray spectra. This conjecture can only be strengthened by improvement or correction of the orginal MND model itself.

ACKNOWLEDGMENTS

The authors acknowledge support from the Swedish National Research council (NFR), the Swedish Institute (SI), and the Wenner-Gren Foundation.

APPENDIX A: HAMILTONIAN

The second quantized Hamiltonian with $a_i^\dagger$ and a_i acting in the HF space reads

$$H=\sum_{ij} h_{ij}a_i^\dagger a_j+\frac{1}{2}\sum_{ijkl}(ji|kl)a_i^\dagger a_j^\dagger a_k a_l,$$

$$(ji|kl)=\int\int dx_1 dx_2 \psi_j^*(1)\psi_i^*(2)r_{12}^{-1}\psi_k(1)\psi_l(2). \tag{A1}$$

The matrix element of the one-electron operator is expressed via the HF one-electron energy ϵ_i,

$$h_{ij}=\epsilon_i\delta_{ij}-\sum_{l<F}[(il|jl)-(il|lj)]. \tag{A2}$$

Then the Hamiltonian takes the form

$$H=\sum_i \epsilon_i a_i^\dagger a_i-\sum_{ij}\sum_{l<F}[(il|jl)-(il|lj)]a_i^\dagger a_j+\frac{1}{2}\sum_{ijkl}(ji|kl)a_i^\dagger a_j^\dagger a_k a_l. \tag{A3}$$

The next step is the selection of the core-electron contribution and taking into account the Coulomb interaction only between the core electron and noninteracting valence electrons. This yields immediately the ND Hamiltonian (5).

APPENDIX B: THE FOURIER TRANSFORM OF THE ND EQUATION

The Fourier transformation[6] of the ND equation (7) and an extraction of the free-particle Green's function give

$$\tilde{\varphi}_n(\epsilon,t)=1+\frac{u_n}{2\pi\iota}\int_{-\infty}^{\infty}d\epsilon_1\left(\frac{1-e^{\iota(\epsilon-\epsilon_1)t}}{\epsilon-\epsilon_1}\right)G_n(\epsilon_1)\tilde{\varphi}_n(\epsilon_1,t),$$

$$\varphi_n(\epsilon,t)=G_n(\epsilon)\tilde{\varphi}_n(\epsilon,t). \tag{B1}$$

It is convenient to rewrite this equation in terms of the advanced Green's function (10) making use of $G_n(\epsilon)=G_A^*(\epsilon)+2\iota\theta(\epsilon_F-\epsilon)\mathrm{Im}\,G_A(\epsilon)$:

$$\tilde{\varphi}_n(\epsilon,t)=1+\frac{u_n}{\pi}\int_{-\infty}^{\infty}d\epsilon_1\tilde{\varphi}_n(\epsilon_1,t)\mathrm{Im}\,G_A(\epsilon_1)\left[\theta(\epsilon_F-\epsilon_1)\times\left(\frac{1-e^{\iota(\epsilon-\epsilon_1)t}}{\epsilon-\epsilon_1}\right)+\frac{e^{\iota(\epsilon-\epsilon_1)t}}{\epsilon-\epsilon_1}\right]+\frac{u_n}{2\pi\iota}\int_{-\infty}^{\infty}d\epsilon_1\tilde{\varphi}_n(\epsilon_1,t)\times\left(\frac{G_A^*(\epsilon_1)-G_A(\epsilon_1)e^{\iota(\epsilon-\epsilon_1)t}}{\epsilon-\epsilon_1}\right). \tag{B2}$$

According to Eq. (11),

$$\tilde{\varphi}_n(\epsilon,t)=a(\epsilon)+b(\epsilon)e^{\iota\epsilon t} \tag{B3}$$

is analytical for $t>0$ in the upper half-plane. The coefficients $a(\epsilon)$ and $b(\epsilon)$ have poles only on the real axes in points where $1+u_n\,\mathrm{Re}\,G_A(E_\alpha^n)=0$. Meanwhile, $\tilde{\varphi}_n(\epsilon,t)$ is finite on the real axis.

This allows to integrate the last term in Eq. (B2): The integration contour is lying in the upper half-plane for the term $\sim G_A^*(\epsilon_1)$ where $G_A^*(\epsilon_1)$ is analytical. The second contribution is integrated over a closed contour in the lower half-plane where $G_A(\epsilon_1)$ is analytical and $\exp(-i\epsilon_1 t)\to 0$ when $\mathrm{Im}(\epsilon_1)\to-\infty$. This results finally in Eq. (9).

[1] L. Triguero, Y. Luo, L. G. M. Pettersson, H. Ågren, P. Väterlein, M. Weinelt, A. Föhlisch, J. Hasselström, O. Karis, and A. Nilsson, Phys. Rev. B **59**, 5189 (1999).
[2] F. Gel'mukhanov and H. Ågren, Phys. Rep. **312**, 87 (1999).
[3] G. D. Mahan, Phys. Rev. **163**, 612 (1967).
[4] P. Noziéres and C. T. De Dominicis, Phys. Rev. **178**, 1097 (1969).
[5] K. Schönhammer and O. Gunnarsson, Solid State Commun. **23**, 691 (1977).
[6] V. I. Grebennikov, Yu. A. Babanov, and O. B. Sokolov, Phys. Status Solidi A **79**, 423 (1977).
[7] V. I. Grebennikov, Yu. A. Babanov, and O. B. Sokolov, Phys. Status Solidi A **80**, 73 (1977).
[8] C.-O. Almbladh and L. Hedin, in *Handbook on Synchrotron Radiation*, edited by D. E. Eastman, Y. Farge, and E.-E. Koch (North-Holland, Amsterdam, 1983), Vol. 1B, p. 607.
[9] G. D. Mahan, *Many-Particle Physics* (Plenum, New York, 1990).
[10] K. Ohtaka and Y. Tanabe, Rev. Mod. Phys. **62**, 929 (1990).
[11] T. Privalov, F. Gel'mukhanov, and H. Ågren, following paper, Phys. Rev. B **64**, 165116 (2001).
[12] U. von Barth and G. Grossmann, Phys. Rev. B **25**, 5150 (1982).
[13] F. Gel'mukhanov and H. Ågren, J. Chem. Phys. **103**, 5848 (1995).
[14] B. I. Lundqvist, Phys. Kondens. Mater. **9**, 236 (1969).
[15] R. Manne and T. Åberg, Chem. Phys. Lett. **7**, 282 (1970).
[16] D. C. Langreth, Phys. Rev. **182**, 973 (1969).
[17] M. Combescott and P. Noziéres, J. Phys. (Paris) **32**, 913 (1971).
[18] J. J. Hopfield, Comments Solid State Phys. **2**, 40 (1969).
[19] D. R. Penn, S. M. Girvin, and G. D. Mahan, Phys. Rev. B **24**, 6971 (1981).
[20] J. Friedel, Comments Solid State Phys. **2**, 21 (1969).
[21] S. G. Rautian and A. M. Shalagin, *Kinetic Problems of Non-Linear Spectroscopy* (North-Holland, Amsterdam, 1991).
[22] F. Gel'mukhanov, P. Salek, A. Shalagin, and H. Ågren, J. Chem. Phys. **112**, 5593 (2000).